Free convection induced by a horizontal wavy surface in a porous medium

1994 Fluid Dyn. Res. 14 151

(http://iopscience.iop.org/1873-7005/14/4/A01)

ELSEVIER

Fluid Dynamics Research 14 (1994) 151–166

FLUID DYNAMICS RESEARCH

Free convection induced by a horizontal wavy surface in a porous medium

D.A.S. Rees[a],

[a]*School of Mechanical Engineering, University of Bath, Claverton Down, Bath, BA2 7AY, UK*

I. Pop[b]

[b]*Faculty of Mathematics, University of Cluj, R-3400, Cluj, CP 253, Romania*

Received 18 November 1993, Revised 22 March 1994

Abstract

The effect of stationary surface waves on the free convection induced by a horizontal uniformly heated surface in a porous medium is studied. Attention is focused on those cases where the waves have an $O(Ra^{-1/3})$ amplitude, where the Rayleigh number, Ra, is based on the wavelength of the waves and is assumed large. Within this amplitude regime the resulting nonsimilar boundary layer flow is described by a set of nonlinear parabolic partial differential equations whose solution is effected by means of the Keller box method.

Extensive computations are presented for a wide range of wave amplitudes and phases, and some global heat transfer rates are given. For all amplitudes and phases a thin near-wall boundary layer develops within the basic boundary layer as the distance downstream increases; an asymptotic analysis is given which determines the structure of this layer. When the wave amplitude is greater than roughly $0.95\ Ra^{-1/3}$ localised regions of reverse flow occur at the heated surface, the number of which depend on the amplitude and phase of the waves.

Nomenclature

a	amplitude of the nonuniform surface
a_1, b_1	numerical values appearing in Eq. (22)
f	reduced streamfunction
F	reduced streamfunction (for near-wall layer)
g	acceleration due to gravity
K	permeability of the porous medium
l	lengthscale associated with the surface waves
L	long lengthscale used in Sect. 4
$\boldsymbol{n}$	unit vector normal to the wavy surface
Ra	$g\beta Kl(T_w - T_\infty)/\nu\kappa$, the Darcy–Rayleigh number based on l

SSDI 169-5983(94)00013-P

s	arc-length along the wavy surface
T	temperature
x, y	streamwise and cross-stream cartesian coordinates
X	slow ξ-variable in Sect. 4
α	scaled wave amplitude
β	coefficient of thermal expansion
η	similarity variable
κ	thermal diffusivity of the saturated medium
θ	dimensionless temperature
Θ	perturbation temperature (near-wall layer)
ν	kinematic viscosity
ψ	streamfunction
ϕ	wave phase
ξ	streamwise coordinate
ζ	near-wall cross-stream coordinate
Superscripts	
$-$	dimensional variables
$\hat{}$	stretched variables ($\xi < 1$)
$\sim$	perturbed variables in Sect. 4
Subscripts	
w	condition at the wall
∞	condition at infinity
0	plane wall similarity solution

1. Introduction

The study of free convection heat transfer from uniform surfaces embedded in a saturated porous medium has attracted a great deal of interest for many investigators over the last two decades; see Nield and Bejan (1992) for a comprehensive review of this topic. Studies have centred on those cases where the thermal boundary conditions allow the use of similarity transformations to reduce the governing boundary layer equations to a system of ordinary differential equations. In general this means that the heated surface is plane. However, in practice, surfaces are sometimes roughened intentionally in order to enhance the heat transfer. Roughened surfaces are encountered in several heat transfer devices such as flat-plate solar collectors and flat-plate condensers in refrigerators. Larger scale surface nonuniformities are encountered in cavity wall insulating systems and grain storage containers. The only papers to date which study the effects of such nonuniformities on thermal boundary layer flow of a Newtonian fluid are those of Moulic and Yao (1989) and Yao (1983). In the parallel field of thermal boundary layers in porous media, which is of interest here, the only papers to date cover convection induced by a vertical surface (Rees and Pop (1994a, b)). In this paper we extend the study to a consideration of the effects of a wavy surface profile on convection induced by a horizontal surface.

We consider the effects of stationary transverse waves on the basic boundary layer flow induced by a uniformly heated horizontal surface for which the resulting flow remains two dimensional. The

Rayleigh number, Ra, is based on the wavelength of the surface waves and it is assumed to be large in order that the boundary layer approximation may be invoked. It is found that the amplitude of the waves must be within an $O(Ra^{-1/3})$ range in order to balance direct and indirect buoyancy forces. Within this amplitude range is found the transition to flow separation. Unlike the corresponding vertical configuration, where the $O(1)$ amplitude waves can be accounted for using a similarity solution, the flow here is described by a parabolic set of partial differential equations whose solution cannot be described in terms of a similarity solution. These equations are solved numerically using the Keller box method (Keller and Cebeci (1971)) for a wide range of wave amplitudes and phases.

In Sect. 2 we derive the nonsimilar boundary layer equations which apply for the present problem. The effects of different wave phases and (moderate) amplitudes on the surface slip-velocity and rate of heat flux are presented in Sect. 3, as are details of global rates of heat transfer. Numerically we find that the flow develops a pronounced near-wall layer as the distance downstream of the leading edge, x, increases. An asymptotic analysis is given in Sect. 4 which shows that this sublayer has a relative thickness which is proportional to $x^{-1/2}$ when $x \gg 1$ within the $O(1)$ range in terms of Ra. For wall amplitudes greater than about $0.95\ Ra^{-1/3}$ the flow separates, or rather, the flow develops one or more regions of reverse flow at the heated surface—these results are given in Sect. 5. The large-x analysis of Sect. 4 is used to show that there can only be a finite number of such separated regions, and that there is no separation for sufficiently large values of x. We discuss the results in Sect. 6.

2. Derivation of the boundary layer equations

Consider a horizontal surface with transverse sinusoidal undulations embedded in a porous medium with constant ambient temperature, T_∞, as shown in Fig. 1. In particular, we assume that the surface profile is given by

$$\bar{y} = \bar{s}(\bar{x}) = \bar{a}\sin(\pi\bar{x}/l - \phi), \tag{1}$$

where $\bar{a}$ is the amplitude of the surface wave, l is a characteristic length associated with the wave and ϕ, the phase of the wave. The temperature of the surface is maintained at the constant value, T_w

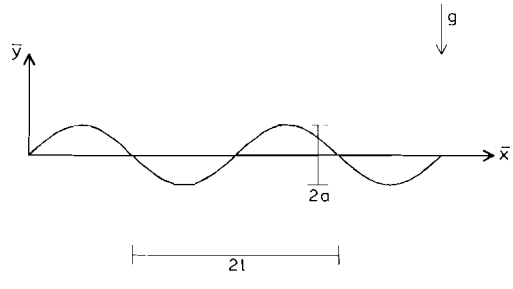

Fig. 1. Physical model and coordinate system depicting transverse surface waves.

which is greater than T_∞. The basic flow is considered to be steady and two-dimensional. All fluid and porous medium properties are assumed to be constant except for the buoyancy term and we assume that the Boussinesq approximation is valid. In terms of dimensionless variables, the Darcy and energy equations can be written as

$$\frac{\partial^2\psi}{\partial x^2} + \frac{\partial^2\psi}{\partial y^2} = -Ra\frac{\partial\theta}{\partial x}, \tag{2}$$

$$\frac{\partial^2\theta}{\partial x^2} + \frac{\partial^2\theta}{\partial y^2} = \frac{\partial\psi}{\partial y}\frac{\partial\theta}{\partial x} - \frac{\partial\psi}{\partial x}\frac{\partial\theta}{\partial y}, \tag{3}$$

where $Ra = g\beta Kl(T_w - T_\infty)/\nu\kappa$ is the Darcy–Rayleigh number based on the temperature drop and the wave lengthscale, l. The boundary conditions which apply are the following:

$$\psi = 0, \quad \theta = 1 \quad \text{on } y = s(x) = a\sin(\pi x - \phi), \tag{4a}$$

$$\partial\psi/\partial y \to 0, \quad \theta \to 0 \text{ as } y \to \infty. \tag{4b}$$

The dimensionless variables are defined as

$$x = \bar{x}/l, \quad y = \bar{y}/l, \quad \psi = \bar{\psi}/\kappa, \tag{5a}$$

$$\theta = (T - T_\infty)/(T_w - T_\infty), \quad a = \bar{a}/l. \tag{5b}$$

Here $\bar{\psi}$ is the dimensional streamfunction which is defined in the usual way. In this paper we restrict attention to those cases for which the nondimensional distance from the leading edge, x, remains $O(1)$ as $Ra \to \infty$ and assume that the wave amplitude of the surface profile, a, is $O(Ra^{-1/3})$: this is, in fact, exactly the order of magnitude of the boundary layer thickness. We note that this condition restricting the maximum amplitude of the waves, and hence the maximum slope, is identical to that employed by Rees and Riley (1985), and Ingham et al. (1985) in their study of convection induced by a near-horizontal plane surface in a porous medium.

The effect of the wavy surface and the invoking of the usual boundary layer scalings are incorporated into the full governing equations by means of the transformation given by

$$x = \xi, \quad y = \xi^{2/3} Ra^{-1/3}\eta + a\sin(\pi\xi - \phi) \tag{6}$$

together with the substitutions

$$\psi = \xi^{1/3} Ra^{1/3} f(\xi, \eta), \quad \theta = \theta(\xi, \eta) \quad \text{and } a = Ra^{-1/3}\alpha. \tag{7}$$

It is straightforward to show that, at leading order in Ra, where $Ra \gg 1$, the following equations are satisfied,

$$f_{\eta\eta} = [2\eta/3 + \alpha\pi\cos(\pi\xi - \phi)\xi^{1/3}]\theta_\eta - \xi\theta_\xi, \tag{8a}$$

$$\theta_{\eta\eta} = \xi(f_\eta\theta_\xi - f_\xi\theta_\eta) - f\theta_\eta/3, \tag{8b}$$

together with the boundary conditions

$$f = 0, \quad \theta = 1 \quad \text{on } \eta = 0, \tag{9a}$$

$$f_\eta, \theta \to 0 \quad \text{as} \quad \eta \to \infty. \tag{9b}$$

As is usual for this class of problem the solution at $\xi = 0$ is obtained by simply setting $\xi = 0$ in Eqs. (8), since all terms involving ξ-derivatives are multiplied by ξ. Furthermore the $\xi = 0$ solution is the plane surface similarity solution. In view of the singular derivative of the $\xi^{1/3}$ term in Eq. (8a) at $\xi = 0$ it was deemed necessary to rewrite Eqs. (8) in terms of the stretched variable $\hat{\xi} = \xi^{1/3}$ when $\xi < 1$. In such cases f and θ satisfy

$$f_{\eta\eta} = [2\eta/3 + \alpha\pi\cos(\pi\hat{\xi}^3 - \phi)\hat{\xi}]\theta_\eta - \hat{\xi}\theta_{\hat{\xi}}/3, \tag{10a}$$

$$\theta_{\eta\eta} = \hat{\xi}(f_\eta\theta_{\hat{\xi}} - f_{\hat{\xi}}\theta_\eta)/3 - f\theta_\eta/3, \tag{10b}$$

and these equations are also subject to the boundary conditions (9).

These two sets of partial differential equations were solved using the now well-known Keller box method (Keller and Cebeci (1991)). Unless otherwise stated in the text the solutions were obtained using a uniform streamwise step of 0.02 in the ξ- or $\hat{\xi}$-directions, and a nonuniform grid of 116 points in the η-direction. We took $\eta_{\max} = 20$, a value well outside the plane surface boundary layer, and concentrated the grid points towards $\eta = 0$. At each step convergence was assumed to have taken place when the maximum absolute change in any quantity was less than 10^{-8}, and double precision arithmetic was used throughout. In general convergence was not difficult to achieve whenever $\alpha < 0.5$, and four Newton–Raphson iterations were usually required to obtain convergence. For larger values of α convergence was assured whenever ϕ lay outside the range from 120° to 150°. Within that small range of phases, solutions beyond $\xi \approx 1$ could not be obtained even with extremely fine grids in the ξ- and/or η-directions.

3. Solutions for moderate amplitudes

In Figs. 2 and 3 are displayed respectively the slip velocity (f_η) and the rate of heat flux (θ_η) at the heated surface ($\eta = 0$) for scaled wave amplitudes, $\alpha = 0$, 0.1, 0.2, 0.3 and 0.4 and phase $\phi = 0°$.

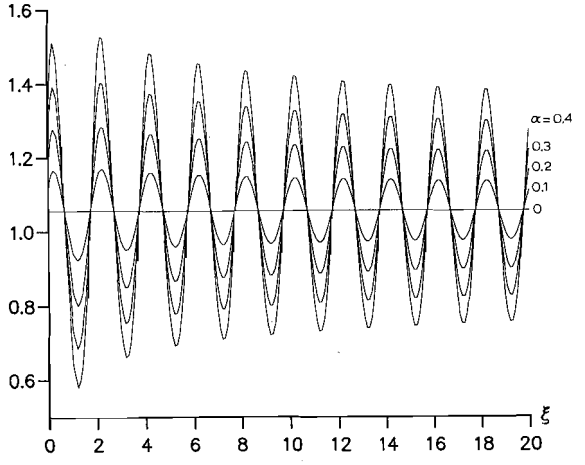

Fig. 2. Variation of the slip-velocity, $f_\eta(\xi, 0)$ with ξ, for wave amplitudes, $\alpha = 0$, 0.1, 0.2, 0.3 and 0.4 and phase, $\phi = 0°$.

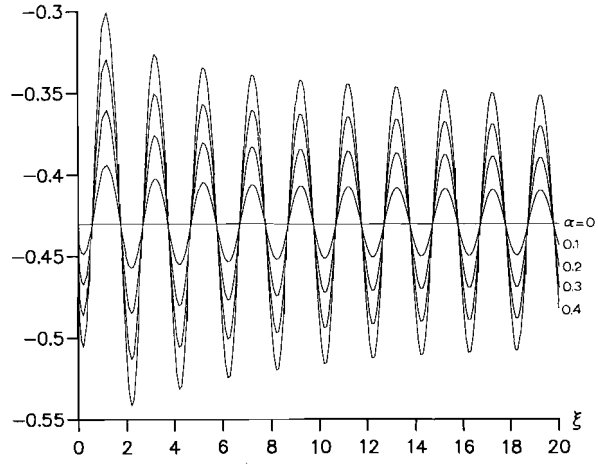

Fig. 3. Variation of the heat flux, $g_\eta(\xi, 0)$ with ξ, for wave amplitudes, $\alpha = 0$, 0.1, 0.2, 0.3 and 0.4 and phase, $\phi = 0°$.

Note that our nondimensionalisation implies that the stationary surface waves have nondimensional period 2. Given that the surface waves have maximum slope at $\xi = 2n$, where n is an integer, it may be seen that slip velocity takes its maximum values just downstream of these positions. Similarly the minimum slip velocity occurs just beyond the positions of minimum slope, $\xi = 2n + 1$. For the vertical counterpart of the present problem such maxima and minima of the slip velocity are precisely at the positions of extreme slope. Although the boundary layer flow is inherently nonlinear, the effects of increasing the wave amplitude can be seen to be roughly linear in terms of its effects on the slip velocity.

The heat flux takes its maxima (minima) at positions just beyond where the waves take their minimum (maximum) slopes. When the slope is positive the usual pressure-gradient mechanism for producing the boundary layer is aided by the additional contribution due to buoyancy forces along the heated surface. This results in the local thinning of the boundary layer and an increased rate of heat transfer. On the other hand the two mechanisms oppose one another when the slope is negative, resulting in a local thickening of the boundary layer and a decrease in the rate of heat transfer. As we will see later flow reversal at the surface does occur when the slope is sufficiently large; to our knowledge this is the first time that flow separation and reattachment has been found for thermal boundary layer flow in porous media.

The effect of varying the phase of the heated surface is given in Fig. 4. Here the scaled wave amplitude is 0.4 and plots are presented for the phases 0°, 90°, 180° and 270°. Of these four cases the maximum positive response is given by the $\phi = 90°$ curve where the configuration corresponds to a precisely horizontal leading edge followed by a section of length 1, the maximum possible length, of positive slope. A similar statement can be made concerning the maximum negative response being related to the negative slope of the boundary when $\phi = 270°$.

Global rates of heat transfer are of interest to the engineer; in Figs. 5–7 we show how this rate varies with distance downstream of the leading edge. Unlike Fig. 3, which shows the *local* rate of

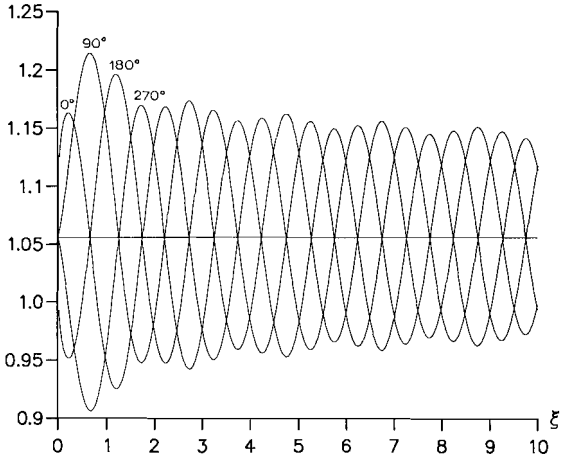

Fig. 4. Variation of the slip-velocity, $f_\eta(\xi, 0)$ with ξ, for wave phases, $\phi = 0°$, $90°$, $180°$, $270°$ and amplitude, $\alpha = 0.4$.

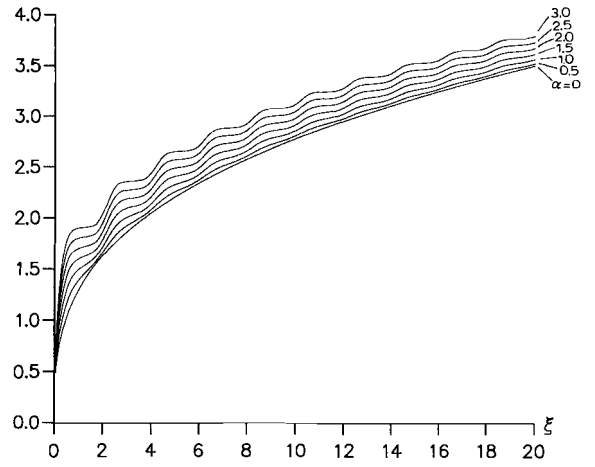

Fig. 5. Global rate of heat transfer, Q, as a function of the downstream distance, ξ, for different wave amplitudes when $\phi = 0°$.

heat transfer, these figures depict the *total* rate of heat transfer obtained by integrating the local rate from the leading edge. Hence the total rate, Q, is given by

$$Q = \int_0^{\bar{x}} (\boldsymbol{n} \cdot \nabla T) \frac{\mathrm{d}\bar{s}(\bar{u})}{\mathrm{d}\bar{u}} \mathrm{d}\bar{u}, \tag{11}$$

where $\boldsymbol{n}$ is the normal to the wavy surface and $\bar{s}(\bar{x})$ is the arc-length along the surface. It is straightforward to show that

$$Q = Ra^{1/3}(T_w - T_\infty) \int_0^{\xi} u^{-2/3} \theta_\eta(u, 0) \mathrm{d}u + \ \ldots\ , \tag{12}$$

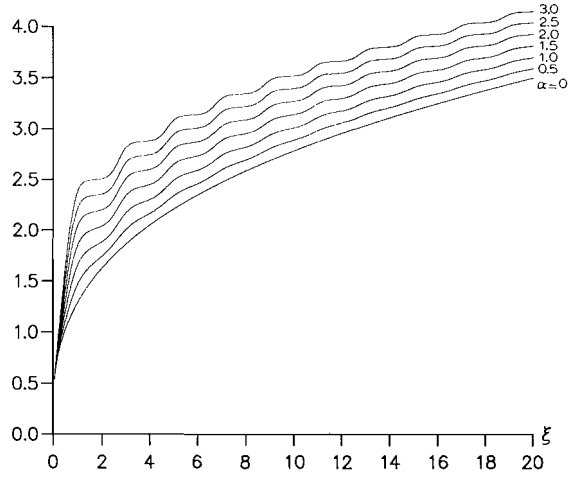

Fig. 6. Global rate of heat transfer, Q, as a function of the downstream distance, ξ, for different wave amplitudes when $\phi = 90°$.

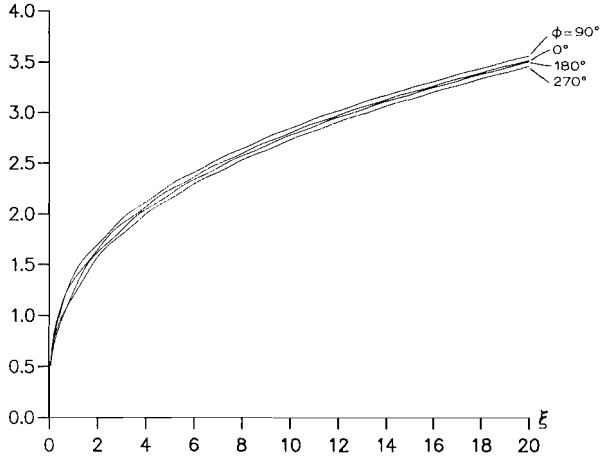

Fig. 7. Global rate of heat transfer, Q, as a function of the downstream distance, ξ, for different wave phases when $\alpha = 0.3$.

when $\theta = \theta(\xi, \eta)$, or when $\theta = \theta(\hat{\xi}, \eta)$,

$$Q = Ra^{1/3}(T_w - T_\infty) \int_0^{\hat{\xi}} 3\theta_\eta(u, 0)\,\mathrm{d}u + \ \ldots\ . \tag{13}$$

Fig. 5 shows how Q varies with ξ for different wave amplitudes when the wave phase is zero. Also shown, for comparison, is the plane-surface result. It is clear that the presence of a wavy surface profile serves to increase the total rate of heat transferred into the medium for this wave phase.

When the wave phase is 90° the corresponding change in the rate of heat transfer is greater; see Fig. 6. For $\phi = 180°$ and $\phi = 270°$ it proves very difficult to obtain solutions for the full range of wave amplitudes and values of ξ shown in Figs. 5 and 6. However, when $\alpha = 0.3$, we see in Fig. 7 that the heat transfer rate is decreased from the plane surface value (not shown), at least for values of ξ greater than roughly 2. Clearly both the amplitude and the phase of the wave are important in determining the precise total rate of heat transfer between the leading edge and some specified point on the wavy surface. But it is evident from examining Figs. 5 and 6 that the 'mean' $\xi^{1/3}$ leading order behaviour is retained. Hence the relative effect of the presence of waves on the total rate of heat transfer is greatest at stations near to the leading edge.

4. Solutions for large distances from the leading edge

In Figs. 2 and 3 we see that the local effect of the surface waves decreases slowly as ξ, the distance from the leading edge, increases. We have investigated this further by integrating the equations for an amplitude $\alpha = 0.3$ and phase $\phi = 0°$ from $\xi = 0$ to $\xi = 50$. The streamlines, isotherms and contours of the function

$$f_\eta(\xi, \eta) - f_\eta(0, \eta), \tag{14}$$

are given in Fig. 8. The effects of the surface waves are clearly seen in the streamline and isotherm plots and can be seen to diminish as ξ increases. From these two plots there would seem to be no evidence for the existence of the thin, near-surface layer mentioned earlier. However, contours of the function given in Eqs. (14) clearly display the developing nature of a near-wall layer and we proceed now to perform an asymptotic analysis for this phenomenon.

First we subtract out the plane wall similarity solution, $f = f_0(\eta)$, $\theta = \theta_0(\eta)$, by setting

$$f(\xi, \eta) = \tilde{f}(\xi, \eta) + f_0(\eta), \tag{15a}$$

$$\theta(\xi, \eta) = \tilde{\theta}(\xi, \eta) + \theta_0(\eta), \tag{15b}$$

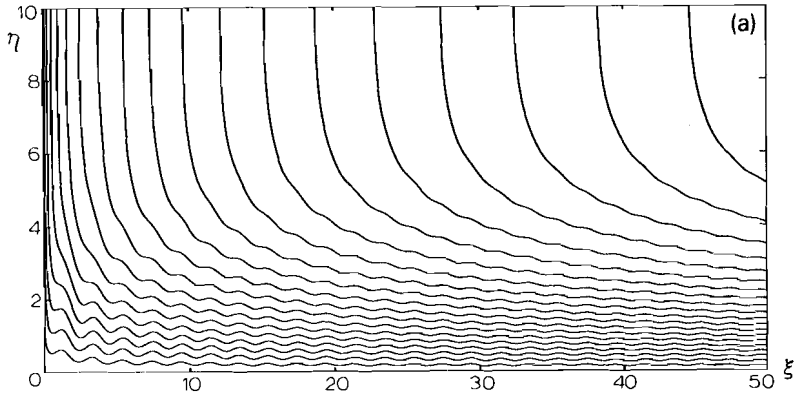

Fig. 8. (a) Streamlines, (b) isotherms and (c) contours of the perturbation slip-velocity, $f_\eta(\xi, \eta) - f_\eta(0, \eta)$, for configuration $\alpha = 0.3$ and $\phi = 0°$. Streamlines are at an interval of 0.5 and isotherms at an interval of 0.05.

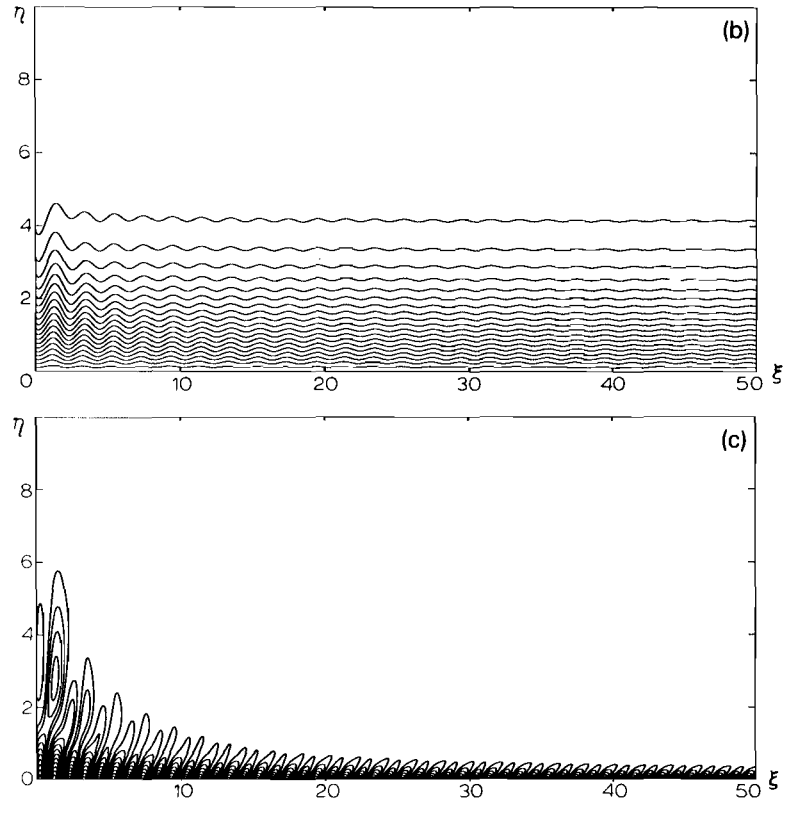

Fig. 8. (Continued).

in Eqs. (8). Secondly, we define X to be a "slow" length scale given by $X = \xi/L$ where $L \gg 1$. The resulting multiple-scale equations are

$$\tilde{f}_{\eta\eta} = [2\eta/3 + \alpha\pi(LX)^{1/3}\cos(\pi\xi - \phi)]\tilde{\theta}_\eta - LX[\tilde{\theta}_\xi + \tilde{\theta}_X/L] + \alpha\pi(LX)^{1/3}\cos(\pi\xi - \phi)\theta_{0\eta}, \tag{16a}$$

$$\tilde{\theta}_{\eta\eta} = XL[(\tilde{f}_\eta + f_{0\eta})(\tilde{\theta}_\xi + \tilde{\theta}_X/L) - (\tilde{f}_\xi + \tilde{f}_X/L)(\tilde{\theta}_\eta + \theta_{0\eta})] - [\tilde{f}\tilde{\theta}_\eta + f_0\tilde{\theta}_\eta + \tilde{f}\theta_{0\eta}]. \tag{16b}$$

Given that $L \gg 1$ the two largest terms in (16a) are

$$-LX\tilde{\theta}_\xi \quad \text{and} \quad \alpha\pi(LX)^{1/3}\cos(\pi\xi - \phi)\theta_{0\eta}. \tag{17}$$

These terms must balance one another and hence, at leading order in L, we obtain

$$\tilde{\theta} = \alpha(LX)^{-2/3}\sin(\pi\xi - \phi)\theta_{0\eta}. \tag{18}$$

To leading order in Eq. (16b) we must have

$$f_{0\eta}\tilde{\theta}_\xi = \tilde{f}_\xi\theta_{0\eta} \tag{19}$$

and hence $\tilde{f}$ is given by

$$\tilde{f} = \alpha(LX)^{-2/3}\sin(\pi\xi - \phi)f_{0\eta}. \tag{20}$$

Thus far, the analysis shows that the streamfunction and temperature should become indistinguishable from their plane surface counterparts fairly quickly since the leading order perturbations decay as $L^{-2/3}$, or equivalently as $\xi^{-2/3}$. However, neither of these expressions for $\tilde{f}$ and $\tilde{\theta}$ satisfy the correct boundary conditions at $\eta = 0$. This problem is overcome by determining a scale for η in terms of L in order that the second η-derivatives in Eq. (16a) and (16b) are retained at leading order. On balancing the $\tilde{f}_{\eta\eta}$ and $LX\tilde{\theta}_{\xi}$ terms in Eq. (16a) we are led to the scaling, $\eta = O(L^{-1/2})$ for large values of L. Setting $\eta = L^{-1/2}\zeta$, $\tilde{f} = L^{-2/3}F$ and $\tilde{\theta} = L^{-2/3}\Theta$ in Eqs. (16a) and (16b) yields the following equations at leading order,

$$F_{\zeta\zeta} = -X\Theta_{\xi} - \alpha\pi b_1 X^{1/3}\cos(\pi\xi - \phi), \tag{21a}$$

$$\Theta_{\zeta\zeta} = X[a_1\Theta_{\xi} + b_1 F_{\xi}], \tag{21b}$$

where $a_1 = 1.055748$ and $b_1 = 0.430213$ (cf. Rees and Bassom [10]) arise in the Taylor series expansion of f_0 an θ_0:

$$f_0(\eta) = a_1\eta + \ \ldots\ , \quad \theta_0(\eta) = 1 - b_1\eta + \ \ldots\ . \tag{22}$$

The solution of Eqs. (21) must satisfy the boundary conditions, $F = \Theta = 0$ on $\zeta = 0$, and should match the solutions (20) and (18), respectively, as $\zeta \to \infty$. These equations are easily solved but the solutions are fairly lengthy to present and are therefore omitted. It should be noted that, although the amplitudes of $\tilde{f}$ and $\tilde{\theta}$ are $O(L^{-2/3})$ for large values of L, the slip velocity and rate of heat flux corresponding to these terms are $O(L^{-1/6})$ since account has to be taken of the near-wall layer variable, ζ, when determining these values. Working back through the various scalings we have introduced eventually gives the following expressions for the slip velocity and rate of heat transfer at the wall surface ($\eta = 0$):

$$f_{\eta} = 1.055748 + (1.154827\alpha/\xi^{1/6})\sin(\pi\xi - \phi + \pi/4) + o(\xi^{-1/6}), \tag{23}$$

$$\theta_{\eta} = -0.430213 - (0.299450\alpha/\xi^{1/6})\sin(\pi\xi - \phi + \pi/4) + o(\xi^{-1/6}), \tag{24}$$

for large values of ξ.

5. Separation and reattachment

In this section we consider the flow which arises for larger values of the scaled wave amplitude, α, than was considered above. When α is sufficiently large (but note that a remains within the $O(Ra^{-1/3})$ range) regions of reverse flow occur. In view of the above arguments concerning the roles of direct and indirect buoyancy forces it is to be anticipated that separation, if it arises in any one particular configuration, will occur when the wave slope is negative. We pursue this aspect numerically in this section and we have used a slightly modified code to obtain the results given

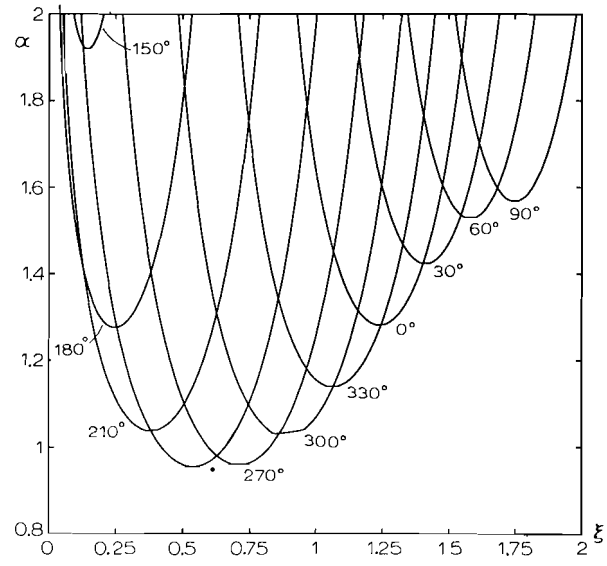

Fig. 9. Positions of separation and reattachment as a function of ϕ for selected values of α.

below. The Keller box code is run from $\xi = 0$ until the value of f_η changes sign. The final steplength is then adjusted iteratively to obtain a zero value of f_η to 6 decimal places. A similar procedure is used to obtain the value of ξ at which reattachment occurs. It is necessary to note that we have not modified the basic Keller-box procedure to integrate through the separated region. The point of separation is regular, as was found by both Rees & Riley (1985) and Ingham et al. (1985) for the case of a near-horizontal heated surface. Numerical experiments confirmed that the weakness of the recirculating regions and their small streamwise extent allowed a safe integration through the separated region, and that the numerical results remain accurate. The Keller-box method becomes numerically unstable when integrating in a more extensive and powerful region of separation.

In Fig. 9 we show the positions of separation and reattachment as a function of ϕ for certain discrete values of α. It is clear from this figure that the first point of separation becomes increasingly close to the leading edge when α increases and $\phi = 180°$. For other values of ϕ the trend is not so straightforward. Taking the $\alpha = 2$ curve, for example, shows us that a decrease in ϕ from 180° eventually results in the sudden disappearance of the region of separation close to $\phi = 150°$. Also plotted on this figure is the locus of those values of ϕ at which separation first occurs and reattachment last occurs for any given wave amplitude; the locus to the left of the bullet symbol, •, denotes separation, while that to the right denotes reattachment. The bullet itself corresponds to where separation and reattachment no longer exist; this corresponds to the values: $\alpha = 0.948$, $\phi = 253.5°$ and $\xi = 0.612$. Thus we conclude that separation cannot occur when α is below 0.948, and may occur above this value only within certain ranges of values of ϕ. An alternative view of Fig. 9 is given in Fig. 10 where the points of separation and reattachment are given as a function of

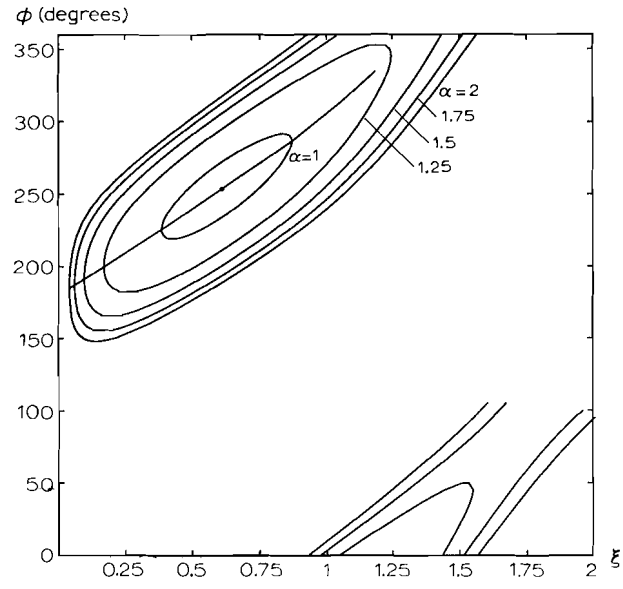

Fig. 10. Positions of separation and reattachment as a function of α for selected values of ϕ.

α for discrete values of ϕ. Again, we mark the point of the first appearance of separation using the bullet symbol.

Given our difficulty in obtaining solutions in the range $120° < \phi < 150°$, as mentioned in Sect. 2, it is worth considering the form Fig. 9 would take should larger values of ξ be used. To answer this question we can use an expression similar to (23) for the slip velocity obtained above. In Fig. 11 we show a *schematic* of where separation occurs using the formula

$$1 + \alpha \sin(\pi\xi - \phi + \pi/4)/(\xi + 1/\xi)^{1/2}, \tag{25}$$

which not only retains the decaying sinusoidal behaviour at large values of ξ but also accounts for a finite cut-off at small values of ξ, unlike Eq. (23) which is strictly valid only for large ξ. Fig. 11 shows that the individual regions of separated flow for any particular phase can be considered to be related to one another by means of changing ϕ smoothly through multiples of 360°. Moreover, in view of the fact that the denominator in the second term in Eq. (25) (and also Eq. (23)) increases as ξ increases, there will always be a distance from the leading edge beyond which separation cannot occur for any given value of α and ϕ and therefore there can only be a finite number of separated regions for any one configuration.

Finally we present a figure showing a case where repeated separation and reattachment occur. In Fig. 12 we show the streamlines and isotherms for the case, $\alpha = 2$ and $\phi = 0°$. The regions of separated flow are clearly evident but their size and strength decrease with each subsequent appearance. Eventually separation ceases to take place, in line with the qualitative analysis

above. Associated with the appearance of separated flow is a substantial enlargening of the boundary layer thickness locally. When the wave slope is negative the rate of heat transfer rises very markedly, as seen by the closeness of the isotherms, but this effect also wanes further downstream.

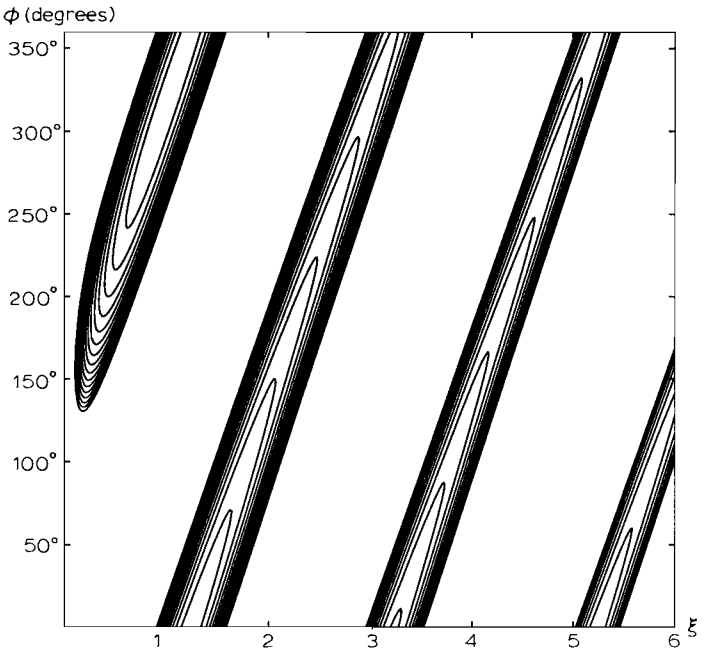

Fig. 11. Schematic corresponding to Fig. 9 showing the qualitative behaviour of the regions of separation using the formula (25).

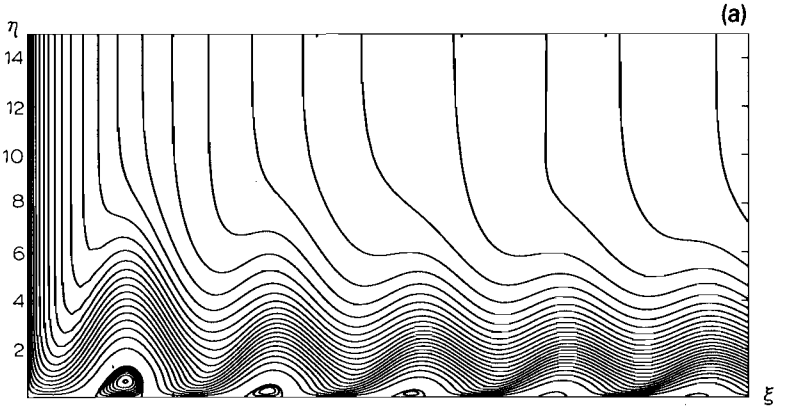

Fig. 12. (a) Streamlines and (b) isotherms for the configuration $\alpha = 2$ and $\phi = 0°$ showing repeated regions of separated flow.

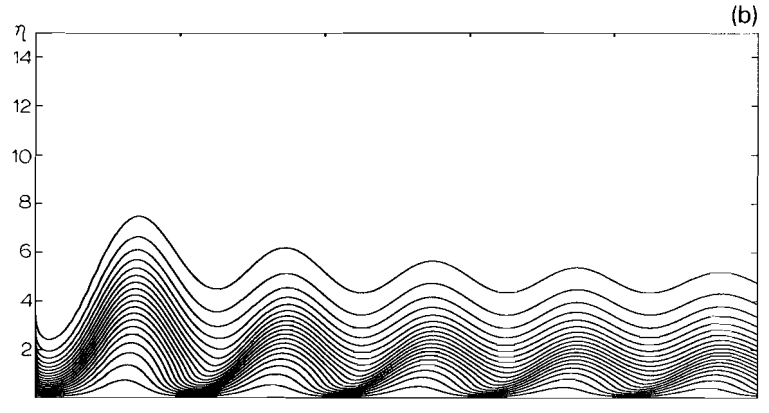

Fig. 12. (Continued).

6. Discussion

We have investigated the effects of a small-amplitude wavy surface profile on the free convective boundary layer flow induced by a constant temperature, horizontally aligned, semi-infinite surface embedded in a porous medium. Results have been presented which give the local slip velocity and heat flux as functions of both the amplitude of the waves, α, and the phase, ϕ, and the qualitative nature of these results are related to the local conditions at the wall. It has been shown that an internal, thin, near-wall layer develops as the distance downstream of the leading edge increases within the $O(1)$ range of values considered here. Strictly speaking, this asymptotic analysis is valid only within the frame-work of the boundary layer scalings, $y = O(Ra^{-1/3})$ and $x = O(1)$ as $Ra \to \infty$. The next step in the study is to relate the large-x lengthscale, L, to some power of Ra in order to obtain an analysis with only one limiting process, and which is valid far downstream of the leading edge. Such an analysis would be equivalent to looking at the effects of small wavelength waves, a configuration more closely related to the study of the effects of surface roughness.

Attention has also been given to the flow resulting from sufficiently large wave amplitudes within the $O(Ra^{-1/3})$ range. Following extensive computations we have delineated those regions where reverse flow occurs and found the wave amplitude below which separation is guaranteed not to occur. Clearly, for asymptotically larger wave amplitudes (with an $O(1)$ wavelength) the present analysis does not apply, but the implication is that regions of separation will persist for substantial distances downstream of the leading edge. For such configurations the present boundary layer scalings are unlikely to apply, and we suspect that, given a sufficiently large wave amplitude, the direct buoyancy forces will be strong enough to produce pairs of boundary layers which collide at each wave crest to form plumes. These plumes would presumably rise in an unsymmetrical manner and deflect away from the leading edge following the overall motion in the positive x-direction.

It is our intention to extend the results of this paper in various directions, one of which is given in the first paragraph of this section. A second extension is to consider the effects of a constant heat flux surface. However, another configuration of great interest is a heated surface with longitudinal waves; preliminary results are available in Rees & Pop (1994c).

Acknowledgements

The first-named author would like to thank the SERC for providing a travel grant which initiated the research undertaken in this paper.

References

Ingham, D.B., J.H. Merkin and I. Pop (1985) Natural convection from a semi-infinite flat plate inclined at a small angle from the horizontal in a saturated porous medium, *Acta Mechanica*, **57**, 183.

Keller, H.B. and T. Cebeci (1971) Accurate numerical methods for boundary layer flows 1. Two dimensional flows, *Proc. Int. Conf. Numerical Methods in Fluid Dynamics*, Lecture Notes in Physics, (Springer, Berlin).

Moulic, S.G. and L.S. Yao (1989), Mixed convection along a wavy surface, *J. Heat Transfer*, **111**, 974.

Moulic, S.G. and L.S. Yao (1989) Natural convection along a vertical wavy surface with uniform heat flux, *J. Heat Transfer*, **111**, 1106.

Nield, D.A. and A. Bejan (1992) Convection in Porous Media (Springer, Berlin).

Rees, D.A.S. and D.S. Riley (1985), Free convection above a near-horizontal semi-infinite surface embedded in a porous medium, *Int. J. Heat Mass Transfer*, **28**, 183.

Rees, D.A.S. and A.P. Bassom, (1991), Some exact solutions for free convective flows over heated semi-infinite surfaces in porous media, *Int. J. Heat Mass Transfer*, **34**, 1564.

Rees, D.A.S. and I. Pop, (1994a) A note on free convection along a vertical sinusoidally wavy surface in a porous medium, to appear in *J. Heat Transfer*.

Rees, D.A.S. and I. Pop (1994b) Free convection induced by a vertical wavy surface with uniform heat flux in a porous medium, to appear in *J. Heat Transfer*.

Rees, D.A.S. and I. Pop (1994c) The effect of longitudinal surface waves on free convection from vertical surfaces in porous media, submitted to *J. Thermophysics and Heat Transfer*.

Yao, L.S. (1983) Natural convection along a vertical wavy surface, *J. Heat Transfer*, **105**, 465.